

Solving Schrödinger equation by meshless methods

H. Montegranario^a, M.A. Londoño^a, J.D. Giraldo-Gómez^a, R.L. Restrepo^b, M.E. Mora-Ramos^c, and C.A. Duque^{d,*}

^a*Instituto de Matematicas, Facultad de Ciencias Exactas y Naturales,
Universidad de Antioquia UdeA, Calle 70 No. 52-21, Medellín, Colombia.*

^b*Universidad EIA, CP 055428, Envigado, Colombia.*

^c*Centro de Investigación en Ciencias-IICBA, Universidad Autónoma del Estado de Morelos,
Av. Universidad 1001, 62209 Cuernavaca, Morelos, Mexico.*

^d*Grupo de Materia Condensada-UdeA, Instituto de Física, Facultad de Ciencias Exactas y Naturales,
Universidad de Antioquia UdeA, Calle 70 No. 52-21, Medellín, Colombia.*

*Phone: +57 4 219 56 30

e-mail: cduque@fisica.udea.edu.co

Received 29 March 2016; accepted 29 April 2016

In this paper we apply a numerical meshless scheme for solving one and two dimensional time independent Schrödinger equation by means of collocation method with Radial Basis Functions interpolants. In particular we approximate the solutions using multiquadrics. The method is tested with some of the well-known configurations of Schrödinger equation and compared with analytical solutions, showing a great accuracy and stability. We also provide some insight on how to use meshless algorithms for obtaining the eigenenergies and wavefunctions of one- and two-dimensional Schrodinger problems.

Keywords: Meshless methods; low dimensional systems; quantum wells; quantum dots; Schrödinger equation.

PACS: 78.67.Hc; 78.67.-n

1. Introduction

During the last two decades there has been an increasing interest toward the solution of different n-dimensional problems by meshless methods. These methods are referred as being applied over scattered data and independent of dimension. They have been found to be widely successful for the interpolation of scattered data. More recently, radial basis functions (RBF) methods have emerged as an important tool for the numerical solution of partial differential equations (PDEs) [1]. RBF's methods can be as accurate as spectral methods without being tied to a structured computational grid. This results in ease of application for the case of complex geometries in any number of space dimensions. This way of solution of PDEs has drawn the attention of many researchers in science and engineering.

One of the first meshless methods, the so-called Kansa's method -developed by Kansa in 1990 [2, 3]-, is obtained by directly collocating the RBFs, particularly the multiquadrics (MQ) one, in the look for the numerical approximation of the solution. Kansa's method was recently extended to solve various ordinary and partial differential equations including the 1D nonlinear Burgers equation [4] with shock wave, shallow water equations for tide and currents simulation [5], heat transfer problems [6], and free boundary problems [7, 8]. In most of the cases, the accuracy of the RBF solution, however, depends heavily on the choice of the so-called shape parameter c in the multiquadric function $\phi(r) = (c^2 + r^2)^{\beta/2}$ or that for β in the Gaussian basis functions $\phi(r) = \exp(-\beta r^2)$. The choice of this optimal value is still under intensive investigation and many authors have investigated the role of this shape parameter. For instance, Carlson and Foley [9] have

shown that it is problem-dependent. Tarwater [10] found that, by increasing c , the Root-Mean-Square (RMS) of the error dropped to a minimum and, then, increased sharply afterwards. In general, as long as c increases, the system of equations to be solved becomes ill-conditioned.

Radial basis function collocation is currently one of the main methods for meshless collocation. They differ from the polynomial basis functions typically applied in classical collocation methods. There are, in principle, two different approaches to collocation using radial basis functions. The symmetric approach relies on Hermite-Birkhoff interpolation in reproducing kernel Hilbert spaces [11] and its application to PDE was first analyzed in [12, 13]. The Asymmetric approach by Kansa [14] that will be used in this paper, has the advantage that less derivatives have to be formed but has the drawback of an asymmetric collocation matrix, which can even be singular in specially constructed situations [15, 16]. Despite this drawback asymmetric collocation has been used frequently and successfully in several applications. Schaback has shown that with some assumptions and modifications it is possible to prevent numerical failure and to prove error bounds and convergence rates [16].

On the other hand, with the development of high-speed computing machines, seeking the numerical solution for the Schrödinger equation has become a subject of great activity. Analytic solutions for Schrödinger equation have been developed and studied extensively in past decades. In more than one dimension, the two main approximate techniques besides the direct solution of relatively few cases via special functions, are the perturbation theory and the variational methods [17]. Many of the closed solutions have been established

using these methods. However, in most cases the use of numerical methods is indispensable, for example, analytical solutions are not possible or become difficult to find in the case of an exciton in a spherical quantum dot system, due to the fact that the corresponding electron and hole effective mass differential equations cannot be uncoupled. Thus, it is important to find numerical alternatives for solving these equations that do not reveal as much demanding when it comes to computer capacity.

In recent decades, a rather large number of numerical methods have been developed for the solution of the Schrödinger-like problem. Among them we can mention the shooting methods [18, 19]; Anderson Monte Carlo [20]; genetic algorithms [21]; and variational methods [21, 22]. Historically, the main approach for the numerical solution of the Schrödinger problem in more than one-dimension has made use of finite difference methods (to know about only a few of them see [23, 24] and references therein). In recent times, some authors have put forward the use of the meshless approach for the solution of the Schrödinger problem in more than one dimension, as an alternative [25]. Within the same spirit, the present work is aimed at providing some insight on the use of meshless algorithms for obtaining the eigenenergies and wavefunctions of one- and two-dimensional Schrödinger equations that can be related with the effective mass description of electron states in low-dimensional semiconductor heterostructures [26]. We organize the article in the following way: In Sec. 2, we introduce meshless methods with the help of the concept of conditionally positive definite functions. In Sec. 3 we give details of the n -dimensional interpolation problem for scattered data. These tools are applied in section four in the numerical solution of Schrödinger eigenvalue problem by collocation of radial basis functions; we explain our algorithm and finally in section five we show the accuracy and application of our method comparing with some well-known analytical solutions of Schrödinger equation.

2. Meshless methods and Radial basis functions

The evolution of what is currently known as meshless methods started around 1950's, closely related to spline theory, in the context of interpolation and approximation of functions [27, 28], inverse problems [29, 30] or computer vision [30–32]. Later, they have been applied to other problems, specially the numerical solution of PDE. Meshless methods are based on radial basis functions interpolators of the form $S : \mathbb{R}^n \rightarrow \mathbb{R}$

$$S(\mathbf{x}) = \sum_{i=1}^M \alpha_i \phi(\|\mathbf{x} - \mathbf{a}_i\|) + p(x), \quad (1)$$

where \mathbf{x} and \mathbf{a}_i belong to \mathbb{R}^n , and \mathbf{a}_i are the interpolation nodes. Besides, $\|\cdot\|$ is the Euclidian norm and $\phi : \mathbb{R} \rightarrow \mathbb{R}$ is a radial basis function. Some well-known choices for $\phi(r)$ are

- (i) Multiquadric $\phi(r) = \sqrt{c^2 + r^2}$
- (ii) Thin Plate Spline (TPS) $\phi(r) = r^2 \log(r)$, and
- (iii) Gaussian $\phi(r) = \exp(-\beta r^2)$.

On the other hand, $p(\mathbf{x})$ is a polynomial term of small degree in n variables. For example, for thin plate spline in \mathbb{R}^2 , $\mathbf{x} = (x, y)$, and $p(\mathbf{x}) = \beta_1 + \beta_2 x + \beta_3 y$. In some cases, $S(\mathbf{x})$ does not have polynomial term as, for example, the multiquadric and the Gaussian radial basis. In accordance, we have the following

Definition 1 A function $\Phi : \mathbb{R}^n \rightarrow \mathbb{R}$ is called radial if there exists a univariate function $\phi : [0, \infty) \rightarrow \mathbb{R}$ such that

$$\Phi(\mathbf{x}) = \phi(r), \text{ with } r = \|\mathbf{x}\| \quad (2)$$

where $\|\cdot\|$ is the Euclidian norm and ϕ is called a radial basis function (RBF).

In spite of the great number of available functions to be considered as radial basis, there is a relatively small number of RBFs that has arisen in the treatment of some particular problems, and constitute the commonly used radial functions in practice. They appear collected in Table I.

Given any function $\Phi : \mathbb{R}^n \rightarrow \mathbb{C}$, and a set of knots or centers $\mathcal{A} = \{\mathbf{a}_1, \dots, \mathbf{a}_M\} \subset \mathbb{R}^n$, we can associate some kind of interpolation matrix \mathbf{A} , whose entries are $A_{jk} = \Phi(\mathbf{a}_j - \mathbf{a}_k)$, together with the quadratic form $\sum_{j=1}^M \sum_{k=1}^M \alpha_j \alpha_k \Phi(\mathbf{a}_j - \mathbf{a}_k)$. The properties of this quadratic form and its application to the approximation problem can be understood with the following definition

Definition 1 A continuous function $\Phi : \mathbb{R}^n \rightarrow \mathbb{C}$ is said to be conditionally positive definite (CPD) of order m on \mathbb{R}^n if

$$\boldsymbol{\alpha}^t \mathbf{A} \boldsymbol{\alpha} = \sum_{j=1}^M \sum_{k=1}^M \alpha_j \alpha_k \Phi(\mathbf{a}_j - \mathbf{a}_k) \geq 0 \quad (3)$$

for any M different points $\mathcal{A} = \{\mathbf{a}_1, \mathbf{a}_2, \dots, \mathbf{a}_M\} \subseteq \Omega \subset \mathbb{R}^n$ and $\boldsymbol{\alpha} = [\alpha_1, \alpha_2, \dots, \alpha_M]^t \in \mathbb{C}^n$, satisfying

$$\sum_{j=1}^M \alpha_j p(\mathbf{a}_j) = 0, \quad (4)$$

for any p in $\Pi_{m-1}(\mathbb{R}^n)$. Where $\Pi_{m-1}(\mathbb{R}^n)$ is the ring of polynomials of n variables of degree less or equal than $m - 1$.

If $\boldsymbol{\alpha}^t \mathbf{A} \boldsymbol{\alpha} > 0$ -provided that the points \mathbf{a}_i are distinct- and $\boldsymbol{\alpha} \neq 0$, we say that the function Φ is strictly conditionally positive definite of order m .

In particular, the case $m = 0$ yields the class of (strictly) positive definite functions. As a consequence of this definition a function which is CPD of order m on \mathbb{R}^n is also CPD of any higher order. Micchelli [33] showed that interpolation with strictly CPD functions of order one is possible even without adding a polynomial term.

TABLE I. The most frequently applied radial basis functions.

Name	RBF	Parameters	order
Linear	$\phi(r) = r$		$m = 1$
Cubic	$\phi(r) = r^3$		$m = 2$
Gaussian	$\phi(r) = e^{-\beta r^2}$	$\beta > 0$	$m = 0$
Poli-harmonic	$\phi(r) = r^\beta$	$\beta > 0, \beta \notin 2\mathbb{N}$	$m \geq [\beta/2]$
Thin plate spline	$\phi(r) = r^\beta \log(r)$	$\beta \in 2\mathbb{N}, \beta > 0$	$m \geq [\beta/2]$
Multiquadric	$\phi(r) = (c^2 + r^2)^{\beta/2}$	$c > 0, \beta \notin 2\mathbb{N}$	$m \geq [\beta/2]$
Inverse multiquadric	$\phi(r) = (c^2 + r^2)^{\beta/2}$	$\beta < 0$	$m = 0$
Wendland Function	$\phi(r) = (1 - r)^4 + (4r + 1)$	$n \leq 3$	$m = 0$

3. The Interpolation Problem

Once the role of radial basis functions as interpolators is understood, the application for solving differential equations is straightforward. In order to properly illustrate, we first give a description of the interpolation issue. Accordingly, the approach to meshless reconstruction is based in the following multivariate interpolation problem:

Given a discrete set of scattered points $\mathcal{A} = \{\mathbf{a}_1, \mathbf{a}_2, \dots, \mathbf{a}_M\} \subset \mathbb{R}^n$ and a set of possible noisy measurements $\{z_1, \dots, z_M\} \subset \mathbb{R}$, find a continuous or sufficiently differentiable function $f : \mathbb{R}^n \rightarrow \mathbb{R}$, such that f interpolates ($f(\mathbf{a}_i) = z_i$) or approximates ($f(\mathbf{a}_i) \approx z_i$) the data $D = \{(\mathbf{a}_i, z_i)\}_{i=1}^M$.

Example 1 Let us apply radial basis functions Eq. (1) to interpolate a surface given in the form $z = f(x, y)$ from the data $\{z_i = f(x_i, y_i)\}_{i=1}^M$ or $D = \{(\mathbf{a}_i, z_i)\}_{i=1}^M$. The coordinates of nodes are given by $\mathbf{a}_i = (x_i, y_i)$, $i = 1, \dots, M$, and the surface is given -just to pick one- by Franke's function (Fig. 1(a)),

$$\begin{aligned}
 f(x, y) = & \frac{3}{4} \exp \left[-\frac{(9x-2)^2}{4} - \frac{(9y-2)^2}{4} \right] \\
 & + \frac{3}{4} \exp \left[-\frac{(9x+1)^2}{49} - \frac{9y+1}{10} \right] \\
 & + \frac{1}{2} \exp \left[-\frac{(9x-7)^2}{4} - \frac{(9y-3)^2}{4} \right] \\
 & - \frac{1}{5} \exp \left[-(9x-4)^2 - (9y-7)^2 \right]. \quad (5)
 \end{aligned}$$

This function has been sampled for nodes in the region $\Omega = [0, 1] \times [0, 1]$ (see Fig 1(d)) with $M=100$. The usual plot of $f(x, y)$ appears in the Fig. 1(a), whereas applying the multiquadric and the Gaussian, $S(\mathbf{x})$ —without polynomial term—to the scattered sample points, it has the form displayed in Figs. 1(b) and 1(c), respectively.

The interpolation conditions $S(\mathbf{a}_i) = z_i, i=1, 2, \dots, M$, produce M equations and the interpolant S is completely determined by the α_i 's after solving the system $\mathbf{A}\alpha = z$, where \mathbf{A} is an interpolation matrix, $\mathbf{A} = [A_{ij}]$, with

$$\begin{aligned}
 A_{ij} &= \phi(\|\mathbf{a}_i - \mathbf{a}_j\|) \text{ with } i, j = 1, \dots, M, \\
 \alpha &= [\alpha_1, \alpha_2, \dots, \alpha_M]^t, z = [z_1, z_2, \dots, z_M]^t. \quad (6)
 \end{aligned}$$

It is possible to observe that the use of RBF interpolation in the reconstruction of the function leads to—essentially—the same graphics as it is were produced by the direct plot of the Franke's function (in all cases we used MATLAB for producing the figures). Although the use of RBF interpolation in this example might be seen as useless, we consider it suitable for highlighting the power of this kind of interpolating schemes.

4. Meshless solutions of Schrödinger equation

As it is known, in quantum mechanics, the state of motion of a particle is specified by giving the wave function, which is—in general—the solution of the *time-dependent Schrödinger equation*. The Schrödinger's equation (SE) is a postulate that constitute the fundamental equation of quantum mechanics. It affirms that the time evolution of a particle of mass m , described by a wave function $\psi(\mathbf{x}, t)$, is linked to the potential in which it is moving by the relation

$$i \hbar \frac{\partial \psi(\mathbf{x}, t)}{\partial t} = \left[-\frac{\hbar^2}{2m} \nabla^2 + V(\mathbf{x}, t) \right] \psi(\mathbf{x}, t). \quad (7)$$

In this partial differential equation $V(\mathbf{x}, t)$ is the local potential operator, which depends of the spatial position $\mathbf{x} = (x, y, z)$ and the time t . In addition, $-(\hbar^2/2m)\nabla^2$ is the kinetic energy operator, where $\nabla^2 \psi = \psi_{xx} + \psi_{yy} + \psi_{zz}$ is the Laplacian operator. The sum of these two latter terms defines what is known as the Hamiltonian operator (or total energy operator) \hat{H} of the particle's motion:

$$\hat{H} = \left[-\frac{\hbar^2}{2m} \nabla^2 + V(\mathbf{x}, t) \right]. \quad (8)$$

The physical state of a particle at time t is completely described by the wave function $\psi(\mathbf{x}, t)$. The probability of finding the particle within a region Ω is

$$\iiint_{\Omega} |\psi|^2 dx dy dz. \quad (9)$$

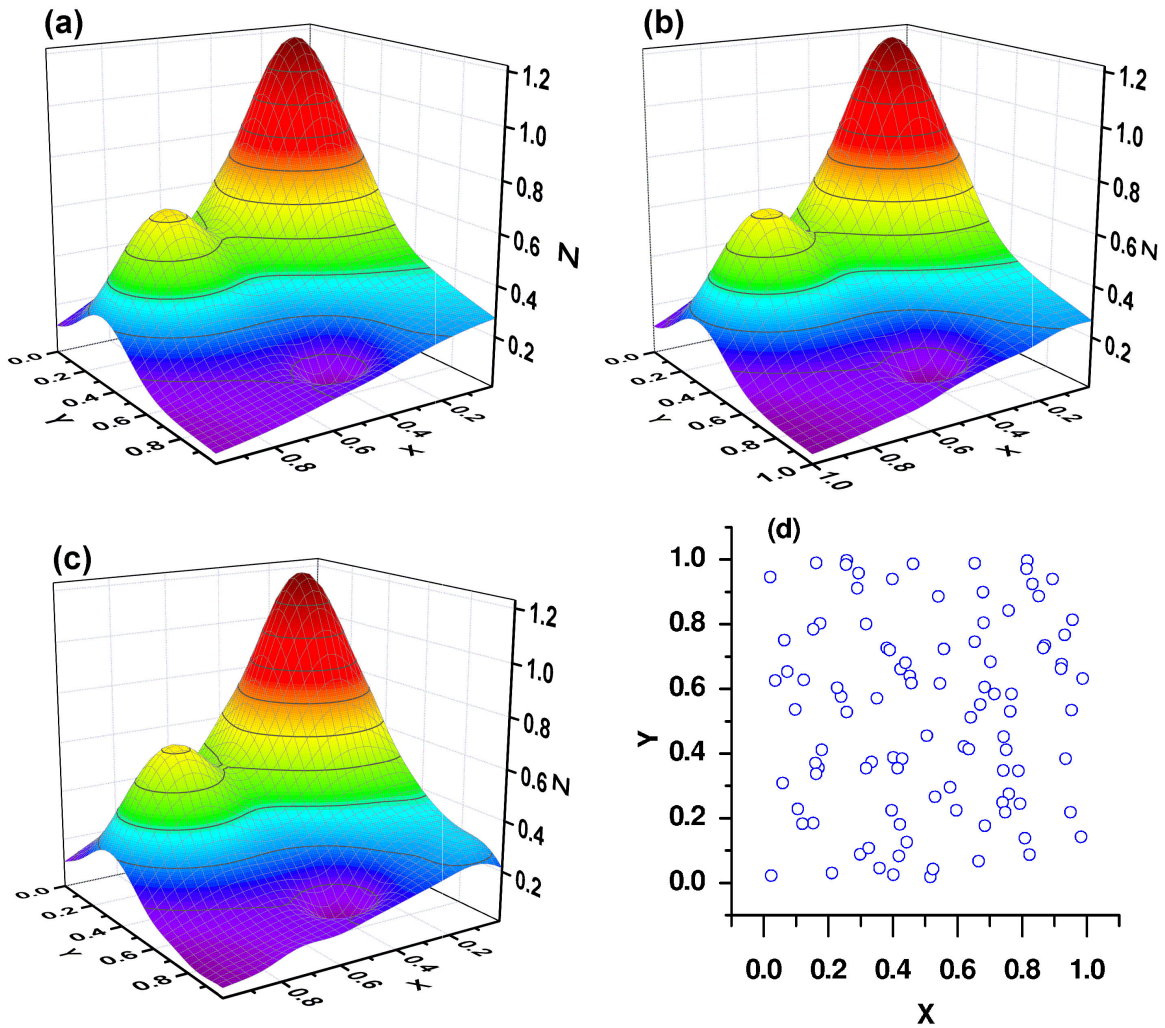


FIGURE 1. Reconstructions of Franke's function: Direct plot of Franke's function (a), Multiquadric reconstruction (b), Gaussian reconstruction (c), and distribution of the scattered points (d).

Since the particle must always be somewhere in the space, the probability of finding the particle within the whole space is one; that is, there is normalization condition that reads

$$\int_{-\infty}^{\infty} \int_{-\infty}^{\infty} \int_{-\infty}^{\infty} |\psi|^2 dx dy dz = 1. \quad (10)$$

Many interesting problems in quantum mechanics do not require considering the SE in its whole generality. Usually, the most interesting states of a quantum system are those in which the system has a definite total energy, and it turns out that for these states the wave function is a standing wave. In other words, the SE predicts that wave functions can form standing waves, called stationary states. When the time-dependent SE is applied to these standing waves, it reduces to a simpler equation called the *time-independent SE*,

$$\nabla^2 \psi + \frac{2m}{\hbar^2} [E - V(\mathbf{x})] \psi = 0. \quad (11)$$

The latter expression can also be written as an eigenvalue problem

$$\hat{H}\psi(\mathbf{x}) = E\psi(\mathbf{x}) \quad (12)$$

It is generally accepted from the early stages of Quantum Mechanics foundation that the determination of the possible eigenvalues, E of the Hamiltonian characteristic Eq. (12) is one of the essential problems of the study of the quantum world. Until today it has not been solved exactly for many physical systems. Even for relatively simple cases –some of which relate with the simulation of the energy band structure of artificially made condensed low-dimensional systems– the exact solution of the stationary SE is not possible with the means of nowadays mathematics. This constitutes a motivation for the use of efficient numerical approaches to obtain it; specially those capable of dealing in a handy way with 2D and 3D domains of complicated geometry. In this sense, it is possible to mention the application of a meshless approach by Dehghdan and Shokri [34].

Radial basis function collocation is currently one of the main methods for meshless collocation. They differ from the polynomial basis functions typically applied in classical

collocation methods. There are, in principle, two different approaches to collocation using radial basis functions. The symmetric approach relies on Hermite-Birkhoff interpolation in reproducing kernel Hilbert spaces [11] and its application to PDE was first analyzed in [12, 13].

The Asymmetric approach by Kansa [14] that will be used in this paper, has the advantage that less derivatives have to be formed but has the drawback of an asymmetric collocation matrix, which can even be singular in specially constructed situations [15, 16]. Despite this drawback asymmetric collocation has been used frequently and successfully in several applications. Schaback has shown that with some assumptions and modifications is possible to prevent numerical failure and to prove error bounds and convergence rates [16].

We now consider a general class of boundary or initial value problems for partial differential equations:

$$\begin{cases} \mathcal{L}u = f, & \text{in } \Omega \\ \mathcal{B}u = 0, & \text{in } \partial\Omega \end{cases} \quad (13)$$

with \mathcal{L} a linear partial differential operator, and \mathcal{B} a linear boundary operator that prescribes values on the boundary of $\partial\Omega$. If we look for a solution for $\mathcal{L}u = f$ such that $u = \sum_{j=1}^N \alpha_j v_j$ in terms of basic functions $\{v_1, v_2, \dots, v_N\}$, then

$$\mathcal{L}u = \sum_{j=1}^N \alpha_j \mathcal{L}v_j = f \quad (14)$$

The collocation method finds an approximate solution to a differential equation evaluating in collocation points $\{\mathbf{a}_i\}_{i=1}^N$, such that

$$\begin{aligned} \mathcal{L}u(\mathbf{a}_i) &= \sum_{j=1}^N \alpha_j \mathcal{L}v_j(\mathbf{a}_i) \\ &= f(\mathbf{a}_i), \quad \text{for } i = 1, \dots, N \end{aligned} \quad (15)$$

is a system of linear equations. Then if we want to solve Eq. (13) with first order absorbing boundary condition

The Asymmetric Kansa's approach assumes an approximate solution of the form

$$u(\mathbf{x}) = \sum_{i=1}^N \alpha_i \phi(\|\mathbf{x} - \mathbf{a}_i\|) \quad (16)$$

For N_I nodes $\{\mathbf{a}_i\}_{i=1}^{N_I} \in \Omega$ in the interior of the domain and N_B nodes $\{\mathbf{a}_i\}_{i=N_I+1}^N \in \partial\Omega$ on the boundary, where $N = N_I + N_B$. The approximated solution is completely determined by finding the scalars $\boldsymbol{\alpha} = [\alpha_1, \alpha_2, \dots, \alpha_N]^t$. In order to obtain $\boldsymbol{\alpha}$, we enforce \mathcal{L} at every point in Ω and \mathcal{B} at every point in $\partial\Omega$

$$\begin{aligned} (\mathcal{L}u)(\mathbf{a}_j) &= \mathcal{L} \left(\sum_{i=1}^N \alpha_i \phi(\|\mathbf{x} - \mathbf{a}_i\|) \right) (\mathbf{a}_j) \\ &= \sum_{i=1}^N \alpha_i \mathcal{L}\phi(\|\mathbf{a}_j - \mathbf{a}_i\|) = f(\mathbf{a}_j), \\ &\text{for } j = 1, 2, \dots, N_I \end{aligned} \quad (17)$$

and

$$\begin{aligned} (\mathcal{B}u)(\mathbf{a}_j) &= \sum_{i=1}^N \alpha_i \mathcal{B}\phi(\|\mathbf{a}_j - \mathbf{a}_i\|) = 0, \\ &\text{for } j = N_{I+1}, N_{I+2}, \dots, N \end{aligned} \quad (18)$$

This leads to the matrix form

$$A = \begin{bmatrix} \mathcal{L}[\phi] \\ \mathcal{B}[\phi] \end{bmatrix} \quad (19)$$

With

$$\begin{aligned} \mathcal{L}[\phi]_{ij} &= \mathcal{L}(\phi)(\|\mathbf{a}_j - \mathbf{a}_i\|), \\ &\text{where } j = 1, 2, \dots, N_i, i = 1, \dots, N \\ \mathcal{B}[\phi]_{ij} &= \mathcal{B}(\phi)(\|\mathbf{a}_j - \mathbf{a}_i\|), \\ &\text{where } j = N_{I+1}, \dots, N, i = 1, \dots, N \end{aligned} \quad (20)$$

And the linear system we have to solve is

$$A\boldsymbol{\alpha} = \begin{bmatrix} \mathbf{f} \\ \mathbf{0} \end{bmatrix} \quad (21)$$

In particular, we are going to apply this scheme for solving the time-independent SE in \mathbb{R}^n ($n = 1, 2$) in the form of an eigenvalue problem with Dirichlet boundary conditions on $\Omega \subset \mathbb{R}^n$

$$\begin{cases} \hat{H}\psi(\mathbf{x}) = E\psi(\mathbf{x}), & \mathbf{x} \in \Omega \\ \psi|_{\partial\Omega} = 0 \end{cases} \quad (22)$$

where $\hat{H} = -\nabla^2 + \tilde{V}(\mathbf{x})$. For sake of numerical simplicity we have omitted the coefficient $\hbar^2/2m$, once we have done this, the units of our numerical findings will be in effective units –for length and energy. The problem (22) usually appears when one looks for the confined energy states in a quantum heterostructure. Thus, we assume an approximation $\psi(\mathbf{x})$ to the solution of the Eq. (22), proposed in the form of radial basis function, without polynomial term

$$\psi(\mathbf{x}) = \sum_{i=1}^N \alpha_i \phi(\|\mathbf{x} - \mathbf{a}_i\|) \quad (23)$$

with N distinct collocation points $\mathcal{A} = \mathcal{A}_\Omega \cup \mathcal{A}_{\partial\Omega}$ and ensuring (22) holds at these points. Evaluating (23) at the collocation points, we have a system of linear equations

$$\psi(\mathbf{a}_i) = \sum_{j=1}^N \alpha_j \phi(\|\mathbf{a}_i - \mathbf{a}_j\|), \quad i = 1, \dots, N. \quad (24)$$

Now, we introduce the notation $\psi_j = \psi(\mathbf{a}_j)$, $\boldsymbol{\psi} = [\psi_1, \psi_2, \dots, \psi_M, \psi_{M+1}, \dots, \psi_N]^t$, $\phi_{ij} = \phi(\|\mathbf{a}_i - \mathbf{a}_j\|)$, and define the matrix

$$A = \begin{bmatrix} \phi_{11} & \phi_{12} & \cdots & \phi_{1N} \\ \phi_{21} & \phi_{22} & \cdots & \phi_{2N} \\ \vdots & \vdots & \ddots & \vdots \\ \phi_{N1} & \phi_{N2} & \cdots & \phi_{NN} \end{bmatrix} \quad (25)$$

such that, according with Eq. (24), it is possible to write

$$\psi = \mathbf{A}\alpha. \quad (26)$$

Here, \mathbf{A} is strictly positive definite. So, it is nonsingular and we can put

$$\alpha = \mathbf{A}^{-1}\psi. \quad (27)$$

On the other side \mathbf{A} can be decomposed in two parts

$$\mathbf{A}_\Omega = \begin{cases} \phi_{ij} & \text{if } 1 \leq i \leq M \text{ and } 1 \leq j \leq N \\ 0 & \text{if } M+1 \leq i \leq N \text{ and } 1 \leq j \leq N \end{cases} \quad (28)$$

and

$$\mathbf{A}_{\partial\Omega} = \begin{cases} 0 & \text{if } 1 \leq i \leq M \text{ and } 1 \leq j \leq N \\ \phi_{ij} & \text{if } M+1 \leq i \leq N \text{ and } 1 \leq j \leq N. \end{cases} \quad (29)$$

Clearly, $\mathbf{A} = \mathbf{A}_\Omega + \mathbf{A}_{\partial\Omega}$. Hence, with (27) and the former notation, one obtains

$$\mathbf{H} = \left(-\nabla^2 \mathbf{A}_\Omega + \mathbf{A}_{\partial\Omega} + \text{diag}([\tilde{V}])\mathbf{A}_\Omega \right) \mathbf{A}^{-1}, \quad (30)$$

where $[\tilde{V}]$ is the vector whose components are the results of the evaluation of the potential function $\tilde{V}(\mathbf{x})$ at the collocation points $\{\mathbf{a}_i\}_{i=1}^M$ $[\tilde{V}] = [\tilde{V}(\mathbf{a}_1), \dots, \tilde{V}(\mathbf{a}_M), 0_{M+1}, \dots, 0_N]$, and

$$\nabla^2 \mathbf{A}_\Omega = \begin{cases} \nabla^2 \phi_{ij} & \text{if } 1 \leq i \leq M \text{ and } 1 \leq j \leq N \\ 0 & \text{if } M+1 \leq i \leq N \text{ and } 1 \leq j \leq N. \end{cases} \quad (31)$$

As a result of this procedure, we finally arrive at

$$\mathbf{H}\psi = E\psi \quad (32)$$

which represents the discretization of the eigenvalue problem associated to the time-independent SE (22).

From a purely mathematical point of view, the Eq. (22) can be solved for any value of the energy E and used to obtain a corresponding discretized wave function $\psi_E(\mathbf{x})$. However, in the particular situation of allowed confined energy states, the wave functions are physically meaningful if they satisfy the boundary condition $\psi_E(\mathbf{x}) \rightarrow 0$ as $\|\mathbf{x}\| \rightarrow \infty$. So, we must check whether or not a solution obtained for some chosen value of E satisfies this asymptotic condition. In our algorithm this property is ensured by looking for solutions that are sufficiently close to zero at the boundary of the region Ω . That is, we require $\|\psi_{\partial\Omega}\| \approx 0$. In other words, we get physically acceptable wave functions $\psi_E(\mathbf{x})$ only for a set of "allowed" discrete values of the energy, E_n ($n = 1, 2, \dots$). In accordance, $\psi_E(\mathbf{x})$ is an eigenfunction of the SE, and E the associated energy eigenvalue.

4.1. The Algorithm

Now we briefly summarize the algorithm proposed for solving the SE in confined condensed quantum systems. Typically, the Schrödinger problem in this kind of structures involves the use of the so-called effective mass and parabolic

approximations which, under the assumption of independent energy bands, leads to the same mathematical form given for the stationary SE in Eq. (8). **INPUT.** A set of collocation points and the potential function \tilde{V} . **OUTPUT.** An eigenfunction $\psi(\mathbf{x}) = \sum_{j=1}^N \alpha_j \phi(\|\mathbf{x} - \mathbf{a}_j\|)$ and energies E (eigenvalues).

The following steps are:

1. Calculate matrix $A_{ij} = \phi(\|\mathbf{a}_i - \mathbf{a}_j\|)$, $i, j = 1, \dots, N$.
2. Calculate $\mathbf{H} = \left(-\nabla^2 \mathbf{A}_\Omega + \mathbf{A}_{\partial\Omega} + \text{diag}([\tilde{V}])\mathbf{A}_\Omega \right) \mathbf{A}^{-1}$.
3. Find eigenvalues and eigenvectors $\psi = [\psi_1, \psi_2, \dots, \psi_N]^t$ in $\mathbf{H}\psi = E\psi$. **Use an eigenvalue solver for non-symmetric matrices.**
4. Among all eigenvectors ψ , to choose those which satisfy the boundary condition $\|\psi_{\partial\Omega}\| \approx 0$.
5. Calculate $\alpha = \mathbf{A}^{-1}\psi$, $\alpha = [\alpha_1, \alpha_2, \dots, \alpha_N]^t$.
6. The eigenfunction or wave function is $\psi(\mathbf{x}) = \sum_{j=1}^N \alpha_j \phi(\|\mathbf{x} - \mathbf{a}_j\|)$.

5. Examples and numerical calculations

In order to show the advantages of the meshless approach introduced in this article we have made the choice of reproducing some pretty well known problems of quantum mechanics in one and two-dimensions. This will allow to compare with existing results, some of them showing analytical solutions. Thus, we leave the study of the energy states in less common structures for a future work. **In all the following examples the inverse multiquadric RBF ($\beta = -1$) will be used.**

Let us first address some of the simplest one-dimensional problems in quantum mechanics. It is worth mentioning that, although they might seem rather academic ones, their use as conduction and valence band bending profile models is pretty much extended in the literature on low-dimensional heterostructures. Among those that have direct analytical solutions we find:

Example 2 The one-dimensional harmonic oscillator.

The simple harmonic oscillator model plays an important role in many areas of physics. It is used in classical and quantum mechanics for a system that oscillates about a stable equilibrium point to which it is bound by a force obeying Hooke's law $F = -kx$. Thus, any particle oscillating about a stable equilibrium point will oscillate harmonically for sufficiently small displacements. An important example of a quantum harmonic oscillator is the motion of ionic cores inside a solid crystal. Each atom has a stable equilibrium position relative to its neighbors and can oscillate harmonically about that position. Another important example is the diatomic molecule, such as HCl, whose two atoms can vibrate harmonically, in and out from one another.

The quantum mechanical motion of the harmonic oscillator is described by the one-dimensional SE with potential energy function $V(x) = 1/2 m^* \omega^2 x^2$ (Here, m^* is the effective mass of the particle). The normalized complete set of eigenfunctions $\psi_n(x)$ for the problem $H\psi = E\psi$ can be expressed in terms of Hermite polynomials $H_n(x)$ [35, 36]. So we can write the Eq. (12), in this case, as

$$\left[-\frac{\hbar^2}{2m^*} \nabla^2 + \frac{1}{2} m^* \omega^2 x^2 \right] \psi(x) = E\psi(x) \quad (33)$$

where ω is the cyclotron frequency.

The analytic eigenfunctions of the Hamiltonian above are given by

$$\psi_n(x) = N_n H_n(\alpha x) \exp\left(-\frac{\alpha^2 x^2}{2}\right), \quad (34)$$

with the corresponding eigenvalues or energy levels

$$E \equiv E_n = (n + 1/2) \hbar \omega, \quad n = 0, 1, 2, \dots \quad (35)$$

Here $\alpha = \sqrt{m^* \omega / \hbar}$ and N_n are the normalization constants.

We have compared these exact analytical solutions with the numerical solutions by meshless method (Table II and Fig. 2), the results obtained for the energy levels are in remarkably good agreement with the exact values.

We define the effective Rydberg for the energy units [$Ry^* = m^* e^4 / (2 \hbar^2 \epsilon^2)$] and the effective Bohr radius for the length units [$a_0^* = \hbar^2 \epsilon / (m^* e^2)$]. Here ϵ is the dielectric constant of the semiconductor material where we are considering the carriers or particles and e is the absolute value of the electron charge. The results in Fig. 2 have been presented in effective units.

Example 3 *Particle confined in a finite double square quantum well (DSQW).*

We now apply the meshless method with multiquadric basis function $\phi(r) = \sqrt{c^2 + r^2}$ to obtaining the numerical solution of the Schrödinger eigenvalue problem, $\hat{H}\psi = E\psi$, in the well-known case of a finite DSQW. This problem describes a non-relativistic quantum particle of mass m^* moving in a quantum well potential defined by the function

$$V(x) = \begin{cases} V_H & \text{if } x \leq -L_d/2 - L_1 \text{ or } x \geq L_d/2 + L_2 \\ V_b & \text{if } |x| \leq L_d/2 \\ 0 & \text{otherwise,} \end{cases} \quad (36)$$

where L_1 and L_2 are the widths of two square wells, which are separated by a potential barrier of length L_d . For the numerical evaluation we have used the effective units, defined

TABLE II. Eigenstates for the one-dimensional harmonic oscillator, given in units of $\hbar\omega$, calculated with $N = 500$ collocation points. The CPU time was 13.1 s.

Energy	Exact	Approx	% Relative error
E_1	0.5	0.500293	0.058650
E_2	1.5	1.500880	0.058650
E_3	2.5	2.501466	0.058650
E_4	3.5	3.502053	0.058650
E_5	4.5	4.502639	0.058650
E_6	5.5	5.503226	0.058650
E_7	6.5	6.503812	0.058650
E_8	7.5	7.504399	0.058650
E_9	8.5	8.504985	0.058650
E_{10}	9.5	9.505572	0.058650

TABLE III. (MM: Meshless method, DM: Diagonalization method) Lowest energy eigenstates of a finite double square quantum well. On the second column there are the values calculated by our algorithm. $N = 500$ interpolation points were included in the calculation, with two of them taken as boundary points. The remaining data are: $L_1 = L_2 = 2.0 a_0^*$, $L_d = 0.6 a_0^*$, $V_H = 40 Ry^*$ and $V_b = 20 Ry^*$. CPU time with MM was 31 s. Energy values appearing in the third column were obtained by the direct diagonalization of the Hamiltonian, using an expansion over the a basis of eigenfunctions of a rectangular quantum well with infinite potential barriers and well width equals to $50 a_0^*$. The Hamiltonian matrix was constructed using 300 terms in the expansion, which guarantees a convergence toward exact energies with an error less than $0.1 Ry^*$ for the lowest 15 confined states [37]. The fourth column contains the relative error in the MM with respect to the DM.

Energy	MM	DM	% Relative error
E_1	1.691919	1.684946	0.413852
E_2	1.792603	1.780250	0.693917
E_3	6.645933	6.618310	0.417378
E_4	7.127742	7.078604	0.694172
E_5	14.43250	14.36718	0.454625
E_6	15.86026	15.74550	0.728822
E_7	24.29272	24.14478	0.612731
E_8	27.65106	27.44785	0.740344

above. In consequence, the problem to solve is given by the following differential equation

$$-\psi''(x) + \tilde{V}(x)\psi(x) = E\psi(x). \quad (37)$$

The calculated lowest eight confined energy levels as well as their corresponding wave functions are shown in Table III and Fig. 3, respectively. All the numerical procedure took 31 seconds of CPU time in an average portable personal computer, using MATLAB. The number of collocation points in the process was $N = 500$, where two of them were taken as boundary ones and another two were placed at the interfaces.

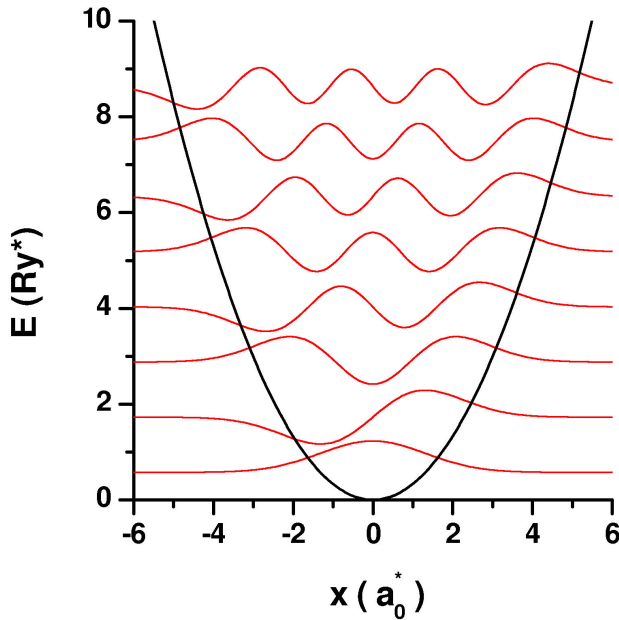


FIGURE 2. Eigenfunctions for the Harmonic oscillator potential. The confinement potential is shown by the parabolic line. Each wavefunction is localized on its corresponding energy. Energies and lengths are given in effective units. Used number of collocation points, $N = 500$. CPU time 13.1 s.

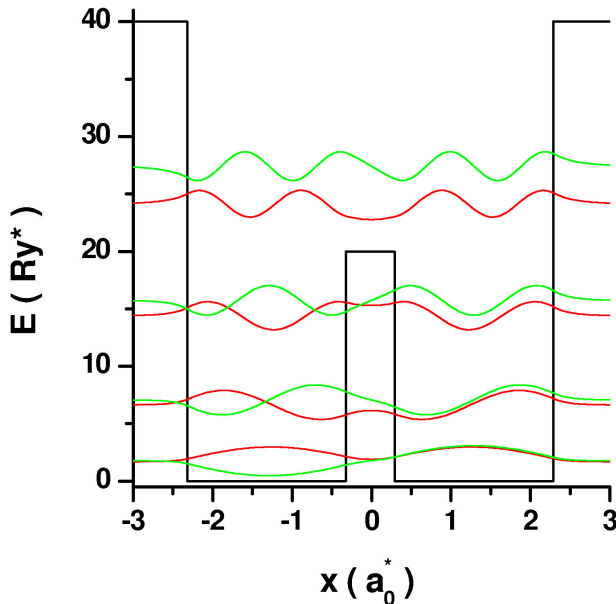


FIGURE 3. Schematic plot of the wave functions corresponding to eigenstates of a finite double square quantum well. Each wave function is placed at the energy corresponding to its eigenvalue. Details are the same as in Table III.

We turn to the solution of the SE in two-dimensional domains. In these cases, for the sake of simplicity, we choose systems with infinite potential barriers. However, this is not a restriction to the method provided finite potential structures can also be calculated by conveniently defining —as it turns out to be often in reality— a boundary $\partial\Omega$, at which the condition of $\psi(\mathbf{x}) \approx 0$ fulfills.

Example 4 *Schrödinger equation for a particle in an isosceles right triangle.* The determination of energy levels and wave functions for a particle confined within different geometric structures in more than one dimension is relevant given the prospective use of these systems in modern technology.

There are some few cases with exact analytical solutions of the Schrödinger problem as it is the case of the one describing the motion of a particle inside a triangle. For a right isosceles triangle those solutions are given in the following conditions. In this two-dimensional problem there is a triangular infinite potential well that confines the particle inside a region determined by the length, L , of the two legs. Then it can be shown that the expressions for the eigenfunctions are [38],

$$\psi'_{mn}(x, y) = \frac{\sqrt{2}}{L} \left[\sin\left(\frac{m\pi x}{L}\right) \sin\left(\frac{n\pi y}{L}\right) + \sin\left(\frac{n\pi x}{L}\right) \sin\left(\frac{m\pi y}{L}\right) \right], \quad (38)$$

for $m = n \pm 1, n \pm 3, \dots$ and

$$\psi''_{mn}(x, y) = \frac{\sqrt{2}}{L} \left[\sin\left(\frac{m\pi x}{L}\right) \sin\left(\frac{n\pi y}{L}\right) - \sin\left(\frac{n\pi x}{L}\right) \sin\left(\frac{m\pi y}{L}\right) \right], \quad (39)$$

for $m = n \pm 2, n \pm 4, \dots$

The corresponding energy levels, in effective units, are

$$E_{mn} = \frac{\pi^2}{L^2}(m^2 + n^2), \quad m, n = 1, 2, 3, \dots, m \neq n. \quad (40)$$

The results obtained by our algorithm with $N = 500$ are in quite good agreement with the values obtained from the corresponding formula, (see Table IV).

Figure 4 contains plots of the two lowest confined states obtained by solving the SE by meshless method and multi-quadratic RBF in the case of a right isosceles triangle with leg

TABLE IV. Eigenenergies, in effective Rydberg units, for a particle confined into a isosceles right triangle. Here the leg length is $L = 4 a_0^*$ and $N = 500$ is the number of collocation points. Used CPU time was 117.6s.

Energy	Exact	Calculated	% relative error
E_{12}	3.084251	3.084473	0.00718
E_{13}	6.168503	6.168499	0.00007
E_{23}	8.019054	8.019916	0.01075
E_{14}	10.48645	10.48526	0.01141
E_{24}	12.33701	12.33712	0.00089
E_{34}	15.42126	15.42279	0.00997
E_{15}	16.03811	16.03387	0.02643
E_{25}	17.88866	17.88617	0.01393
E_{35}	20.97291	20.97232	0.00280

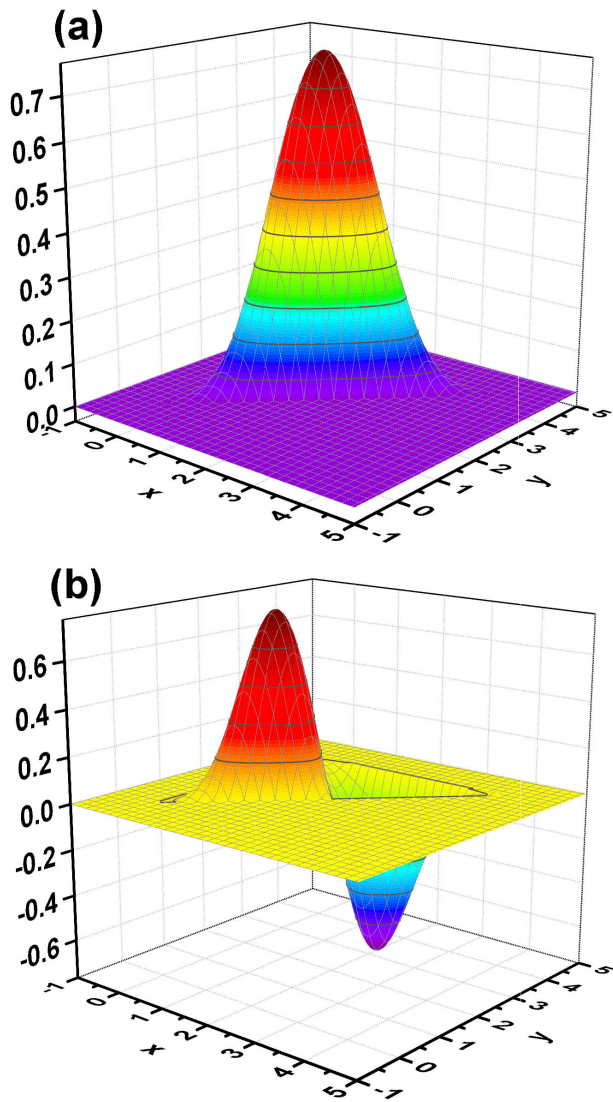


FIGURE 4. Numerical solutions for the wave functions of the two lowest energy states of a particle confined within a isosceles right triangle computed by interpolation methods [39], with data obtained using our algorithm. The scale is given in effective units.

equals to $L = 4 a_0^*$. At this point, some important remarks are worth to be pointed out: i) the differential equation in 2D is solved with a number of $N = 500$ collocation points. ii) with this number of points we need to obtain the wave functions, so one proceeds to perform the interpolation scheme (1), arriving to a grid of 10201 points. iii) with this, we achieve the sufficient smoothness in the resulting functions, in such a way that ulterior integration processes involving them may become accurate enough.

The density plot of the wave functions of the calculated lowest eight energy eigenstates appear in the left-hand column of the Fig. 5, the corresponding densities of probability are shown in the central column.

On the other hand, right-hand column of the Fig. 5 shows the absolute error of the calculated solutions of the 2D SE

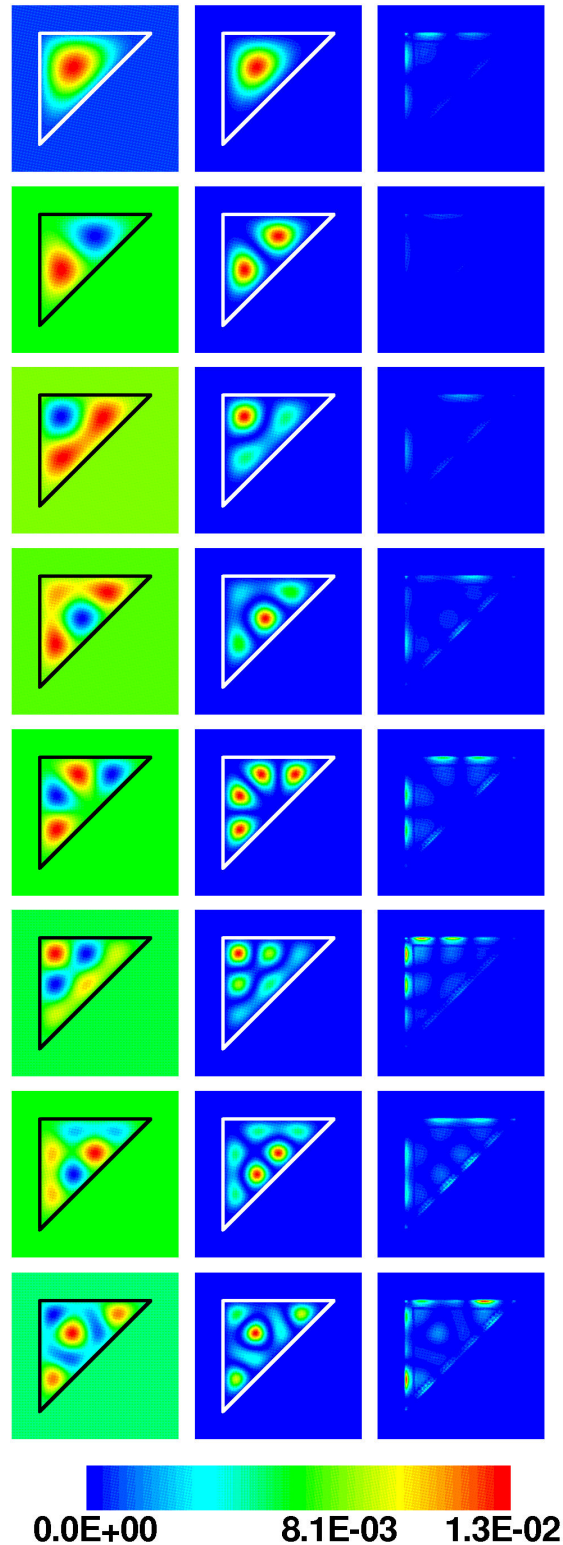


FIGURE 5. Density plots for wave functions (left-hand panel) and their corresponding density of probability (central panel) associated to the first eight eigenenergies of a particle into a isosceles right triangle with infinite confinement potential. Density plot of absolute error between calculated and analytical density of probability for the first eight eigenfunctions (right-hand panel). The color bar in the bottom belongs to the right-hand panel.

equation, corresponding to the energy levels reported in Table IV, with respect to the exact analytical expression of Eqs. (35) and (36). We can see, in all cases, that the lack of coincidence is, at most, of the order of 10^{-2} , with the higher accuracy being obtained for the lowest energy states. This is an indication that the numerical approach is pretty well accurate. In general the boundaries of the region present some difficulties to interpolants, since their reconstruction requires a precise spatial control over the smoothing properties of the radial basis function. Larger errors appear in regions close to the border triangle legs, and that is a consequence of a smaller density of points on the boundary and also of the global smoothness of radial basis interpolants.

Example 5 Particle in an infinite quantum disc.

The two-dimensional infinite quantum disc is defined by the confinement potential function

$$V(r) = \begin{cases} 0, & 0 \leq r \leq R \\ \infty, & r > R, \end{cases} \quad (41)$$

where $r = (x^2 + y^2)^{1/2}$. Inside the disc region the well known analytical $\psi(r, \theta)$ functions that fulfill the boundary conditions $\psi(r = R, \theta) = 0$ are given by using the Bessel functions, which depend on two independent integer quantum numbers m and n . They are given by (see [40])

$$\psi(r, \theta) = N_{m,n} J_m(k_{m,n} r/R) \exp(im\theta), \quad (42)$$

where $N_{m,n}$ are the normalization constants, $m = 0, \pm 1, \pm 2, \dots$ and $k_{m,n}$ is the n -th zero of the function $J_m(r)$, with $n = 1, 2, 3, \dots$. Or, more conveniently, for bound states

$$\psi^-(r, \theta) = J_m(k_{m,n} r/R) \sin(m\theta) \quad (43)$$

and

$$\psi^+(r, \theta) = J_m(k_{m,n} r/R) \cos(m\theta), \quad (44)$$

with eigenenergies, in effective units, given by

Energy	Exact	Calculated	% relative error
E_{10}	1.44580	1.445826	0.00170
E_{11}	3.67050	3.670222	0.00757
E_{11}	-	3.670589	0.00243
E_{12}	6.58338	6.592981	0.14583
E_{12}	-	6.592982	0.14583
E_{20}	7.61782	7.615506	0.03038
E_{13}	10.1766	10.17449	0.02081
E_{13}	-	10.17451	0.02062
E_{21}	12.3046	12.29767	0.05651
E_{21}	-	12.29890	0.04651

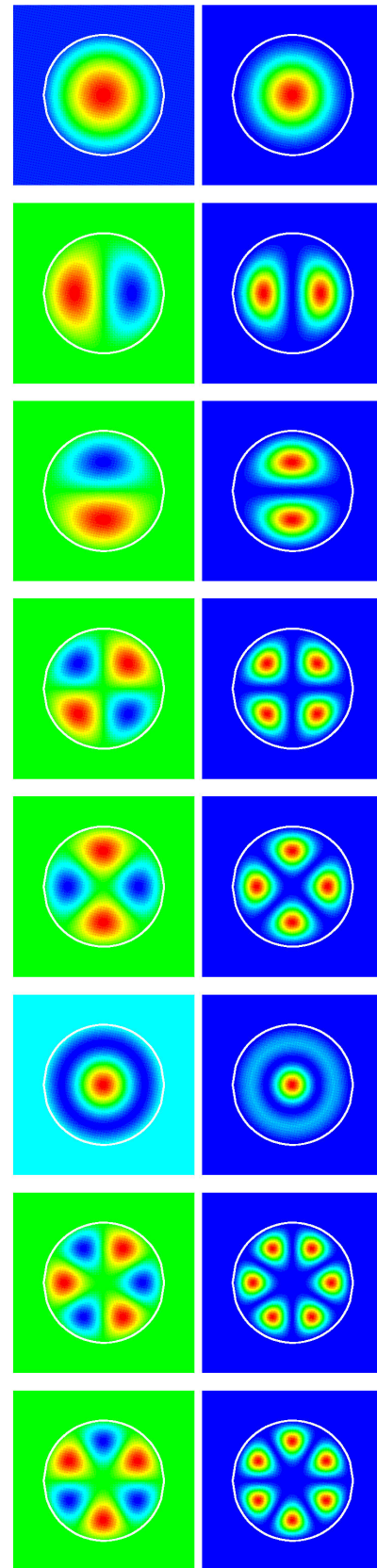


FIGURE 6. Eigenenergies from a particle with infinity confining within a circle of radius $R = 2a_0^*$. The algorithm was performed with $N = 500$ interpolation points.

$$E_{m,n} = \frac{k_{m,n}^2}{R^2}. \quad (45)$$

The numerical results obtained by our algorithm are remarkably similar to the analytical solutions, and are depicted in Table V for a quantum disc of radius $R = 2a_0^*$. Again, the coincidence of the eigenvalues is significantly good. **Note that the largest errors for the obtained wavefunctions correspond to the boundary regions. This could be mitigate by increasing the number of boundary points [1].** Given the symmetry, the calculation in this case has only included $N = 500$ collocation points.

In the Fig. 6 we are presenting the density plots of the confined wavefunctions that correspond to the energy states reported in Table V (left-hand column) as well as the associated probability densities (right-hand column). It is possible to notice that the particular symmetries of the different states are correctly reproduced.

6. Conclusions and future research

We have addressed the subject of solving the Schrödinger equation in one- and two-dimensional problems using a meshless method. The procedure of implementing the numerical procedure has been thoroughly presented. For the sake of comparison, we chose some well known examples for the application of this approach which have, in general, analytical exact solutions. In all cases, the use of the meshless method leads to a remarkably good qualitative and quantitative agreement. In this paper we have used Multiquadric, a globally supported radial basis, the same as thin plate splines and many others. The main disadvantage of globally supported RBFs is that their associated interpolation matrix is full. As a consequence, there exists an upper limit in the number of collocation points of globally supported RBF collocation methods. If the distance between collocation points

is very small, the matrix will become very ill-conditioned, leading to serious numerical singularity and degradation in numerical accuracy. These problems can be avoided by using compactly supported RBFs, and this is a subject of future investigation. That opens the possibility of using this kind of numerical schemes to the study of electron states –and related physical properties– in quantum nanostructures of more complicated or even non-regular geometries. Another possible application is the self-consistent solution of the Schrödinger and Poisson equations in problems with selective doping or polarization-induced charge densities.

A straightforward extension of our approach will be the study of quantum states in three-dimensional confined structures such as quantum dots. The results of such a work will be published elsewhere.

Acknowledgments

This research was partially supported by Colombian Agencies: CODI-Universidad de Antioquia (Estrategia de Sostenibilidad de la Universidad de Antioquia and projects: “Propiedades ópticas de impurezas, excitones y moléculas en puntos cuánticos autoensamblados” and “On the way to development of new concept of nanostructure-based THz laser”), Facultad de Ciencias Exactas y Naturales-Universidad de Antioquia (CAD-exclusive dedication project 2015-2016), and El Patrimonio Autónomo Fondo Nacional de Financiamiento para la Ciencia, la Tecnología y la Innovación, Francisco José de Caldas. RLR is grateful to the Universidad EIA for its financial support through EIA-UdeA project “Efectos de láser intenso sobre las propiedades ópticas de nanoestructuras semiconductoras de InGaAsN/GaAs y GaAlAs/GaAs”. CAD and RLR are grateful to UdeA-EIA-UdeM for financial support through the project: “Propiedades opto-electrónicas de sistemas altamente confinados: Una aproximación teórica”.

1. G. F. Fasshauer, *Meshfree Approximation Methods with MATLAB*, World Scientific Publishing Co., New York (2007).
2. E.J. Kansa, *Computers & Mathematics with Applications* **19** (1990) 127.
3. E.J. Kansa, *Computers & Mathematics with Applications* **19** (1990) 147.
4. Y.C. Hon and X.Z. Mao, *Appl. Math. Comput.* **95** (1998) 37.
5. Y.C. Hon, K.F. Cheung, X.Z. Mao, and E.J. Kansa, *J. Hydraulic Eng.* **125** (1999) 524.
6. M. Zerroukat, H. Power, and C. S. Chen, *Int. J. Numer. Meth. Eng.* **42** (1998) 1263.
7. Y.C. Hon and X. Z. Mao, *Financial Eng.* **8** (1999) 31.
8. M. Marcozzi, S. Choi, and C. S. Chen, *Appl. Math. Comput.* **124** (2001) 197.
9. R.E. Carlson and T.A. Foley, *Comput. Math. Appl.* **21** (1991) 29.
10. A.E. Tarwater, *A parameter study of Hardy's multiquadric method for scattered data interpolation*, Lawrence Livermore National Laboratory, (1985).
11. Z. Wu, *Approximation Theory Appl.* **8** (1992) 1.
12. C. Franke and R. Schaback, *Adv. Comput. Math.* **8** (1998) 381.
13. C. Franke and R. Schaback, *Appl. Math. Comp.* **93** (1998) 73.
14. E.J. Kansa, *Eng. Anal Boundary Elements.* **31** (2007) 577.
15. G.E. Fasshauer, *Meshfree Approximation Methods with MATLAB*. World Scientific (2007).
16. S.I.A.M Schaback, *J. Numer. Anal.* **45** (2007) 333.
17. S. Flügge, *Practical Quantum Mechanics*, Springer, Berlin (1998).

18. M.V. Vener, O. Kühn, and J. Sauer, *J. Chem. Phys.* **114** (2001) 240.
19. M.V. Vener and N. D. Sokolov, *Chem. Phys. Lett.* **264** (1997) 429.
20. J.B. Anderson, *J. Chem. Phys.* **63** (1975) 1499.
21. D.E. Makarov and H. Metiu, *J. Phys. Chem. A* **104** (2000) 8540.
22. B.W. Shore, *J. Chem. Phys.* **59** (1973) 6450.
23. L. Gong, Y.-Ch. Shu, J.-J. Xu, Q.-Sh. Zhu, and Zh.-G. Wang, *Superlatt. Microstruct.* **60** (2013) 311.
24. L. Gong, Y.-Ch. Shu, J.-J. Xu, and Zh.-G. Wang, *Superlatt. Microstruct.* **61** (2013) 81.
25. X.G. Gong, L.H. Shen, D.E. Zhang, and A.H. Zhou, *J. Comput. Math.* **26** (2008) 310.
26. P. Harrison, *Quantum Wells, Wires and Dots: Theoretical and Computational Physics of Semiconductor Nanostructures*, Wiley, Chichester (2010).
27. R.L. Hardy, *J. Geophys. Res.* **76** (1971) 1905.
28. J. Duchon, *Splines minimizing rotation invariant seminorms in Sobolev spaces*, Lecture Notes in Math. **571**, Springer, Berlin (1977).
29. R. Franke, *A critical comparison of some methods for interpolation of scattered data*, Naval Postgrad. School Tech. Report NPS-53-79-003 (1979).
30. D. Marr, *Vision: A Computational Investigation into the Human Representation and Processing of Visual Information*, Freeman, New York (1982).
31. G. Wahba, *Spline models for observational data. (CBMS-NSF Regional Conference Series in Applied Mathematics)*. SIAM: Society for Industrial and Applied Mathematics (1990).
32. D. Terzopoulos, *Multiresolution Computation of Visible-Surface Representations*, Ph.D. Dissertation, Dept. of Electrical Engineering and Computer Science, Massachusetts Institute of Technology, Cambridge, MA, January (1984).
33. C.A. Micchelli, *Constructive Approximation* **2** (1986) 11.
34. M. Dehgdan and A. Shokri, *Comp. Math. Appl.* **54** (2007) 136.
35. S. Weinberg, *Lectures on Quantum Mechanics*. Cambridge University Press (2012).
36. T. Myint-U and L. Debnath, *Linear Partial Differential Equations for Scientists and Engineers*, Birkhauser (2006).
37. M. de Dios-Leyva, C.A. Duque, and L. E. Oliveira, *Phys. Rev. B* **76** (2007) 075303.
38. W.-K. Li, *J. Chem. Educ.* **61** (1984) 1034.
39. H. Montgranario and J. Espinoza, *Variational Regularization of 3D Data: Experiments with MATLAB*, Springer Briefs in Computer Science (2014).
40. R.W. Robinnet, *Quantum Mechanics*, Univesity Press, Oxford (2006).